

## Three-dimensional numerical ray tracing on a phenomenological ionospheric model

L.-C. Tsai,<sup>1,2</sup> C. H. Liu,<sup>3</sup> and J. Y. Huang<sup>1</sup>

Received 14 January 2010; revised 21 June 2010; accepted 29 July 2010; published 22 October 2010.

[1] In this paper we present a numerical and step by step ray-tracing method on a phenomenological ionospheric electron density ( $N_e$ ) model, the TaiWan Ionospheric Model (TWIM), which is constructed from the FormoSat3/Constellation Observing System for Meteorology, Ionosphere and Climate (FS3/COSMIC) ionospheric radio occultation data. With the Earth's magnetic field and horizontal  $N_e$  gradient effects included, efficient methods for calculating ray parameters such as the ground range, reflection height, phase path, and group path are presented. The three-dimensional TWIM consists of vertically fitted  $\alpha$ -Chapman-type layers, with distinct F2, F1, E, and D layers, for which the layer parameters such as peak density, peak density height, and scale height are represented by surface spherical harmonics. This way the continuity of  $N_e$  and its derivatives is maintained. This is important for practical schemes for providing reliable radio propagation predictions. The methodology is successfully applied to a practical high-frequency transmitter for oblique incidence ray tracing and further evaluated by comparing synthetic vertical ionograms generated by the method with experimental ionosonde observations.

**Citation:** Tsai, L.-C., C. H. Liu, and J. Y. Huang (2010), Three-dimensional numerical ray tracing on a phenomenological ionospheric model, *Radio Sci.*, 45, RS5017, doi:10.1029/2010RS004359.

### 1. Introduction

[2] Since the early days of radio wave communications, high frequency (HF) has been extensively used for long-distance radio service, despite the difficulties due to the varying ionospheric structures. HF radio ray tracing in the ionosphere mainly involves refraction and reflection due to ionospheric structure on a large scale compared with the radio wavelength. The tracing results can be efficiently evaluated through the estimated parameters of ground range, reflection height, phase path, and group path. Ray tracing has applications in operation frequency and power management and prediction of HF broadcasting or communication systems as well as in experimental studies on over-the-horizon radar systems and direction finding systems. For these beyond line-of-sight systems their performance depends critically on accurately tracing the ray through a realistic ionospheric

model. Some works of ray tracing have combined scattering and the time varying nature of the ionosphere and provided the additional parameters of field strength, absorption, and Doppler shift, but a detailed discussion is beyond the scope of this study.

[3] The theory of HF radio waves in the ionospheric plasma started early by different groups working on full wave theory [Försterling, 1942; Rydbeck, 1944; Budden, 1952] and geometrical optics [Poevlein, 1948, 1949; Hines, 1951; Haselgrove, 1955]. Since then, two main types of ray tracing in the ionosphere emerged: numerical and analytic. Bennett *et al.* [2004] have discussed and reviewed the theoretical basis and a number of applications and techniques of ray tracing. Over all, the most widely distributed numerical ray-tracing program is probably that developed by Jones [Jones, 1966]. The Jones program provides for a number of models of ionospheric  $N_e$  distribution and the Earth's magnetic field. Reilly [1991] also developed a three-dimensional numerical ray-tracing program which is especially applied to point-to-point propagation and homing-in calculation using approximate partial derivatives of latitude and longitude with respect to launch angle. There are other numerical ray-tracing programs that have been adopted by different groups. However, they are not necessarily freely available. The analytic tracing mostly applies to

<sup>1</sup>Center for Space and Remote Sensing Research, National Central University, Chung-Li, Taiwan.

<sup>2</sup>Institute of Space Science, National Central University, Chung-Li, Taiwan.

<sup>3</sup>Academia Sinica, Taipei, Taiwan.

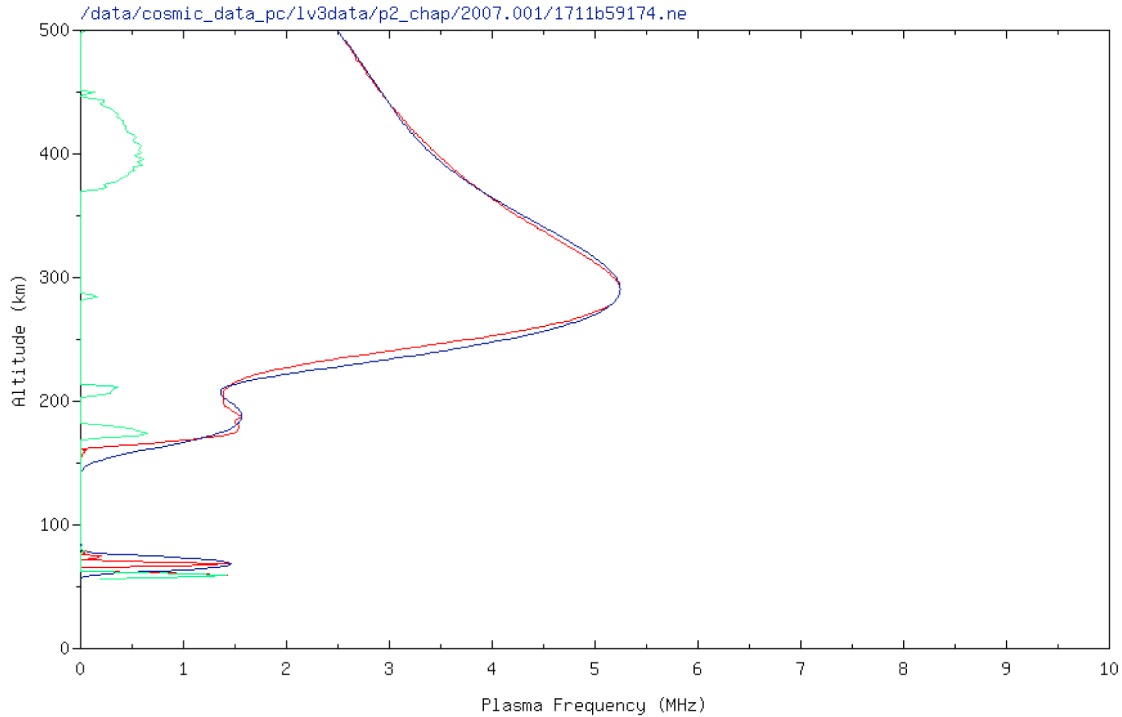


**Figure 1.** An example of daytime  $N_e$  profile fitting, which shows the original RO  $N_e$  profile in red and the fitted  $\alpha$ -Chapman layer profile in blue, and the absolute residual  $N_e$  profile in green. The corresponding  $N_e$  is converted to plasma frequency ( $f_n$ ) for wave propagation applications in accordance with the conversion formula  $f_n^2$  (MHz) =  $80.6 N_e$  (cm $^{-3}$ ).

spherically symmetrical ionospheres where the vertical structures are reconstructed by a choice of suitable functions. Thus the ray-tracing parameters can be efficiently and analytically calculated, and the analytic tracing methods, more properly, are closed-form methods. For a typically analytic method, *Norman and Cannon* [1997] introduced a segmented method for analytic ray tracing (SMART) on the fully analytic ionospheric model (FAIM) [Anderson et al., 1989] and with the Earth's magnetic field. SMART is able to accurately trace the ray by segmenting the ionosphere horizontally as well as vertically and, hence, including horizontal  $N_e$  gradient effects are included. Analytic ray-tracing techniques are much faster than numerical approaches, but they are more restricted in the ionospheric models to which they can be applied.

[4] Here we have attempted to present another numerical and stepped ray-tracing method on a phenomenological ionospheric  $N_e$  model constructed from the FS3/COSMIC data. The primary propose of this construction is to provide subsidiary ray-tracing results through a simple and easily accessible ionospheric  $N_e$

model for applications in communication and wave propagation. The phenomenological ionospheric model provides temporal and synoptic variations in three-dimensional (latitude, longitude, and altitude)  $N_e$  and maintains the continuity in the first and second  $N_e$  derivatives for providing reliable radio propagation predictions and electrostatic field determinations. The concentrations of  $N_e$  at certain altitudes have characteristic maximum peaks, forming the ionospheric F2, F1, E, and D layers. Herein we report the results of ray-tracing parameters of ground range, reflection height, phase path, and group path at conditions with or without an Earth-centered magnetic dipole and horizontal  $N_e$  gradients.

## 2. FS3/COSMIC RO Observations and the TaiWan Ionospheric Model

[5] The FS3/COSMIC program includes six spacecraft (FM1 to FM6) located at a nearly circular orbit of  $\sim 800$  km altitude,  $\sim 70^\circ$  inclination angle, and  $60^\circ$  separation to

receive the Global Positioning System (GPS) signals. The GPS radio occultation (RO) technique has been used to receive multichannel GPS carrier phase signals at low Earth orbiting (LEO) satellites performing active limb sounding of the Earth's atmosphere and ionosphere. Generally FS3/COSMIC can obtain over 2500 RO measurements per day, providing the atmospheric and/or ionospheric data including areas over the oceans and the southern hemisphere, where few ground-based stations are located. For further details about the FS3/COSMIC program, see [Rocken *et al.*, 2000; Hajj *et al.*, 2000]. Each GPS RO observation consists of a set of limb-viewing links with tangent points ranging from the LEO satellite orbit altitude to the Earth's surface. The path TEC values are obtained from differential GPS phase measurements using both the L1 and L2 radio signals at frequencies of 1575.42 MHz and 1227.60 MHz, respectively. The  $N_e$  values at tangent points' radial distances can be retrieved from the calibrated or compensated TEC values [Schreiner *et al.*, 1999; Tsai *et al.*, 2009a] using the Abel integral transform given by Tricomi [1985] and in a recursive way starting from the outmost ray at the LEO orbital altitude to the bottom of the ionosphere. The terrestrial ionosphere at all latitudes has a tendency to separate into layers at different altitude regions. Specifically, the  $N_e$  profiles exhibit layered structures, with distinct F2, F1, E, and D layers, despite the fact that different physical processes dominate in different latitudinal region. In the TWIM each layer is generally characterized by an  $\alpha$ -Chapman function described by the parameters of peak  $N_e$  ( $N_{e\max}$ ), peak density height ( $h_m$ ), and scale height ( $H$ ), and the layer parameters can be obtained with least squares error fitting of the observed profile to the  $\alpha$ -Chapman functions.

$$N_e(\theta, \lambda, h) = \sum_{i=1}^4 N_{e\max}^i(\theta, \lambda) \cdot e^{\frac{1}{2} \left( 1 - \frac{h-h_m^i(\theta, \lambda)}{H^i(\theta, \lambda)} - e^{-\frac{h-h_m^i(\theta, \lambda)}{H^i(\theta, \lambda)}} \right)} \quad (1)$$

where each  $i$  means a physical layer of F2, F1, E, or D layer. An  $\alpha$ -Chapman-type layer is predicted by a simplified aeronomic theory, assuming photoionization in a one-species neutral gas, deionization in recombination, and neglecting transport processes. All of the layers are usually present during the daytime. The F1 and D layers decay at night and could be hidden within the other layers, but the F1 and D layer parameters are still derivable throughout all times by least squares error

fitting. Figure 1 shows an example of daytime  $N_e$  profile fitting and its results. It is noted that the profiles have been normalized to a F2 layer peak density height being equal to 290 km. As shown in Figure 1, unreasonable negative  $N_e$  values could happen at lower F region and/or E region when the retrieval error is accumulated and larger from top to bottom during a standard Abel inversion.

[6] In the TWIM, we assume the ionosphere to be steady state and electrostatic, and a two-dimensional (latitude and longitude) numerical map to fit derived layer peak  $N_e$ , peak density height, or scale height values can be represented by a function  $\Gamma(\theta, \lambda)$  and constructed by spherical harmonic analysis of the Laplace's partial differential equation. Following the work of Jones and Gallet [1962] to present the geographic variations of F2 layer critical frequency, a worldwide mapping in a special form of Legendre functions is applied to values of each layer parameter, and the resulting functions of  $\theta$  (colatitude) and  $\lambda$  (longitude or the local time angle) are combinations of the surface spherical harmonics [Davis, 1989] defined by

$$\Gamma(\theta, \lambda) = \sum_{m=0}^3 \sum_{n=0}^{q_m} [A_{nm} U_{nm}(\theta, \lambda) + B_{nm} V_{nm}(\theta, \lambda)],$$

where

$$U_{nm}(\theta, \lambda) = \sqrt{\frac{2n+1}{2\pi} \frac{(n-m)!}{(n+m)!}} P_n^m(\cos \theta) \cos m\lambda, \quad \text{and}$$

$$V_{nm}(\theta, \lambda) = \sqrt{\frac{2n+1}{2\pi} \frac{(n-m)!}{(n+m)!}} P_n^m(\cos \theta) \sin m\lambda$$

$$(n = 0, 1, 2, \dots, q_m; m = 0, 1, 2, \text{ or } 3), \quad (2)$$

and  $P_n^m()$  is the familiar associated Legendre polynomial of the first kind of degree  $n$  and order  $m$ . After the optimization analyses of noise separation we determined the cutoffs to be an order of 3 and a degree of 20 for each order. For details concerning the performance and evaluation of the TWIM, the interested readers are referred to Tsai *et al.* [2009b]. It is noted that the TWIM is a three-dimensional and continuous model and the continuity of the first and second derivatives for the practical schemes

**Figure 2.** A descriptive flowchart of the complete ray-tracing process from a specified transmitting position to the ground or a maximum altitude.

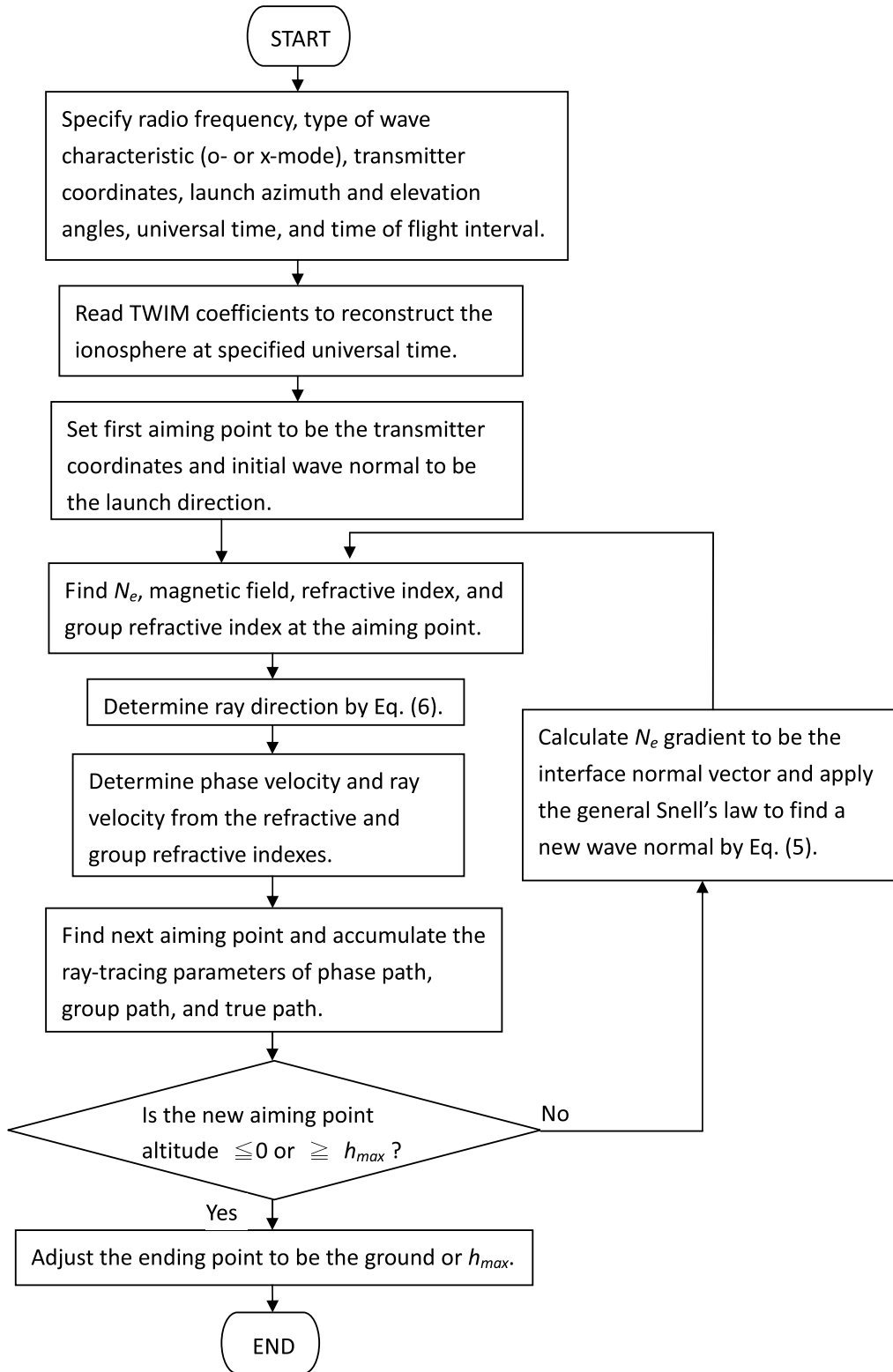


Figure 2

can be maintained. The three spherical components of  $N_e$  gradients are given by

$$\begin{aligned} \frac{\partial N_e}{\partial h} &= \sum_{i=1}^4 N_{e\max}^i \cdot e^{\frac{1}{2}(1-x_i-e^{-x_i})} \cdot \left(-\frac{1}{2} + \frac{1}{2}e^{-x_i}\right) \cdot H^i, \\ \frac{1}{r} \frac{\partial N_e}{\partial \theta} &= \frac{1}{r} \cdot \left[ \sum_{i=1}^4 e^{\frac{1}{2}(1-x_i-e^{-x_i})} \cdot \frac{\partial N_{e\max}^i}{\partial \theta} \right. \\ &\quad \left. + \sum_{i=1}^4 N_{e\max}^i \cdot e^{\frac{1}{2}(1-x_i-e^{-x_i})} \cdot \left(-\frac{1}{2} + \frac{1}{2}e^{-x_i}\right) \cdot \left(-\frac{1}{H^i} \frac{\partial h_m^i}{\partial \theta} - \frac{h-h_m^i}{H^{i2}} \frac{\partial H^i}{\partial \theta}\right) \right] \\ \frac{1}{r \sin \theta} \frac{\partial N_e}{\partial \lambda} &= \frac{1}{r \sin \theta} \cdot \left[ \sum_{i=1}^4 e^{\frac{1}{2}(1-x_i-e^{-x_i})} \cdot \frac{\partial N_{e\max}^i}{\partial \lambda} \right. \\ &\quad \left. + \sum_{i=1}^4 N_{e\max}^i \cdot e^{\frac{1}{2}(1-x_i-e^{-x_i})} \cdot \left(-\frac{1}{2} + \frac{1}{2}e^{-x_i}\right) \cdot \left(-\frac{1}{H^i} \frac{\partial h_m^i}{\partial \lambda} - \frac{h-h_m^i}{H^{i2}} \frac{\partial H^i}{\partial \lambda}\right) \right], \end{aligned} \quad (3)$$

where  $x_i = (h - h_m^i)/H^i$ , and  $i$  means one of the F2, F1, E, and D physical layers. In this study, we use the  $N_e$  gradient to present the refractive-index surface normal, which plays a vital role in the propagation of radio waves. More detail descriptions of the ray-tracing scheme will be presented in section 3.

### 3. Ray-Tracing Scheme and Parameters

[7] Wave propagation can be described by a complicated solution to the Maxwell's equations but, in the case of HF radio waves propagating in a nonabsorbing ionosphere, a geometric optics approach is adequate for ray tracing. Upon incident on a TWIM modeled ionosphere and at each step of the ray tracing, the  $N_e$  values and  $N_e$  gradients at the intersected positions can be determined with the TWIM at specified universal time (UT). Meanwhile, the Earth's magnetic field is assumed to be proportioned to  $1/r^3$  with an Earth centered dipole. Therefore, this study deals with the propagation of plane waves in a slowly varying anisotropic ionosphere. A full three dimensional ray tracing is simulated upon independent vectors of initial ray direction,  $N_e$  gradient, and magnetic field. The start point for this ray-tracing development is the Fermat's principle of least stationary time, i.e., a ray between two points is the path such that the optical path length has a stationary value. In an anisotropic medium this principle can be expressed in the form [Bremmer, 1949]

$$\delta \int n_r ds = \delta \int \mu \cos \alpha ds = 0, \quad (4)$$

where  $n_r$  is the ray refractive index,  $\mu$  is the phase refractive index of nonabsorbing ionosphere,  $\alpha$  is the

angle between the wave vector and the ray direction, and  $ds$  is an element of arc length along the raypath. Next, applying the Euler-Lagrange equations, we derive a generalized differential form of Snell's law [Kelso, 1964] and the corresponding wave normal number  $u$  and its unit vector  $\hat{u}$  can be obtained as follows:

$$\frac{d}{dP}(\mu \hat{u}) = \frac{1}{u} \nabla \mu, \quad (5)$$

where  $P$  is the phase path. Since we are dealing with an anisotropic ionosphere with the Earth's magnetic field but without losses due to collisions, the refractive index  $\mu$  is given by the Appleton-Lassen or the Appleton-Hartree formula [Appleton, 1932; Hartree, 1931], which represents the two magnetoionic modes of ordinary and extraordinary characteristic waves. This paper will include families of rays and contributions associated with both modes. Meanwhile, we assume that the refractive index gradient coincides with the  $N_e$  gradient. In the presence of a non-uniform magnetic field the two gradients should differ, but the effect is always less than  $10^{-4}$  radian at ionospheric heights and can be neglected [Lawrence and Posakony, 1961], although it would have to be included for ray tracing in the exosphere. The ray is situated in the plane defined by the wave normal and the Earth's magnetic field [Bremmer, 1949] and has the angle  $\alpha$  from the wave normal to the ray direction as

$$\tan \alpha = \pm \frac{(\mu^2 - 1)Y \sin \Theta \cos \Theta}{\left[Y^2 \sin^4 \Theta + 4(1 - X)^2 \cos^2 \Theta\right]^{0.5}}. \quad (6)$$

The + and – signs refer to the ordinary-mode (o-mode) and extraordinary-mode (x-mode) waves, respectively,  $X = f_N^2/f^2$  where  $f_N$  is the plasma frequency and  $f$  is the radio frequency,  $Y = f_H/f$  where  $f_H$  is the gyrofrequency, and  $\Theta$  is the angle between  $\hat{u}$  and the Earth's magnetic field.

[8] The scheme of ray tracing is sufficiently complicated that the logical structure will be explained as follows with the aid of the descriptive flowchart shown in Figure 2. The process proceeds start from specifying a set of radio frequency, type of o- or x-mode wave characteristic, transmitter or receiver position, launch or arriving azimuth and elevation angles for forward or backward ray tracing, respectively, initial universal time of ray tracing, and time of flight interval. From the specified ray-tracing universal time, the corresponding surface spherical harmonics coefficients of TWIM are read to reconstruct a three-dimensional ionosphere. Once the launch or arriving azimuth and elevation angles of a ray have been specified, ray tracing begins from a known transmitter or receiver being the initial aiming point, and the wave vector of the beginning path step can be determined. For convenience, assume that the ray is traveling straight along each short step distance within a constant time of flight and then enters a new path step. The ray-tracing scheme presented here calculates integration steps of equal length in an independent variable of elapsed group path (or time of flight). It induces the step size changes required in true path, because, especially near the ray-tracing reflector, when the ray geometry is changing more slowly at an equal length of group path than true path. Through a TWIM modeled ionosphere and an Earth-centered-dipole magnetic model the  $N_e$ , magnetic field, refractive and group refractive indexes at each aiming point can be determined, and then a ray direction is obtained from equation (6) and from one path step to the next. After each step along the path is traced, the new aiming ray position is computed by adding the distance vector to the old aiming position. The step distance is determined by the product of time step and the ray velocity (or packet velocity), the magnitude of which is defined by

$$v_r = \frac{c}{\mu' \cos \alpha}, \quad (7)$$

where  $c$  is the light speed in free space, and  $\mu'$  is the real group refractive index and can be determined by the equations published by *Shinn and Whale* [1952]. Onto the new step, a TWIM  $N_e$  gradient is calculated to be the interface normal vector, and the general Snell's law is applied to derive a new wave vector from equation (5). As the ray could be up through the ionosphere or reflected and back down to the ground the ray tracing process is repeated step by step with equal length in elapsed group path. We note that it is clearly more effi-

cient for the time of flight interval to be large, however, one needs to limit the truncation error. A value of  $10^{-5}$  s has been used in this study.

[9] If a wave is modulated with narrowband modulation, the ground range, reflection height, and true path can be scaled or integrated out from the ray trace directly. For practical HF broadcast or communication, the bandwidth is usually limited by channel dispersion and interference and has so far not exceeded a few kilohertz. The phase path  $P$  of the propagating wave is calculated by accumulating along the ray when the phases of appropriate plane waves propagate in a series of infinitesimal path steps of homogeneous plasma. The group path  $P'$  can be determined by the product of the light speed and the total time of flight which is the sum or integral of the stepped times of flight along the ray. The total phase path and the group path are expressed by

$$P = \int_{ray} \mu \cos \alpha \, ds \cong \sum_i \mu_i \cos \alpha_i \Delta s, \quad (8)$$

and

$$P' = \int_{ray} \mu' \cos \alpha \, ds \cong c \sum_i \Delta t_i. \quad (9)$$

It is noted that the principle of stationary phase can also yield the Fermat's variational equation as shown in equation (4).

#### 4. Ray-Tracing Results and Evaluation by the Chung-Li Dynasonde Observations

[10] To discuss the effects of horizontal  $N_e$  gradient and the Earth's magnetic field, Figure 3 shows ray-tracing paths for various elevation angles of radio waves into a TWIM modeled ionosphere for the cases of zero horizontal  $N_e$  gradient and magnetic field (Figure 3, top) and considering the horizontal  $N_e$  gradients from the TWIM and the Earth's magnetic field (Figure 3, bottom). The ray traces are projected on to both the  $y$ - $z$  (meridional and vertical) and  $x$ - $z$  (longitudinal and vertical) planes and with background imaging colors representing the modeled plasma frequencies from the TWIM at 0400 UT on 15 August 2008. The radio frequencies are all the same 6.5 MHz, and the ten paths for each set correspond to the ten launch elevations from  $90^\circ$  down to  $45^\circ$  in steps of  $5^\circ$ . The transmitter was placed at Chung-Li ( $24.97^\circ\text{N}$ ,  $121.19^\circ\text{E}$ ), Taiwan, and ray tracing was carried out due south. It may be noted that only one set of rays are shown in Figure 3 (top) because of zero magnetic field, and Figure 3 (bottom) shows ordinary and extraordinary ray separation when ray tracing includes the Earth's

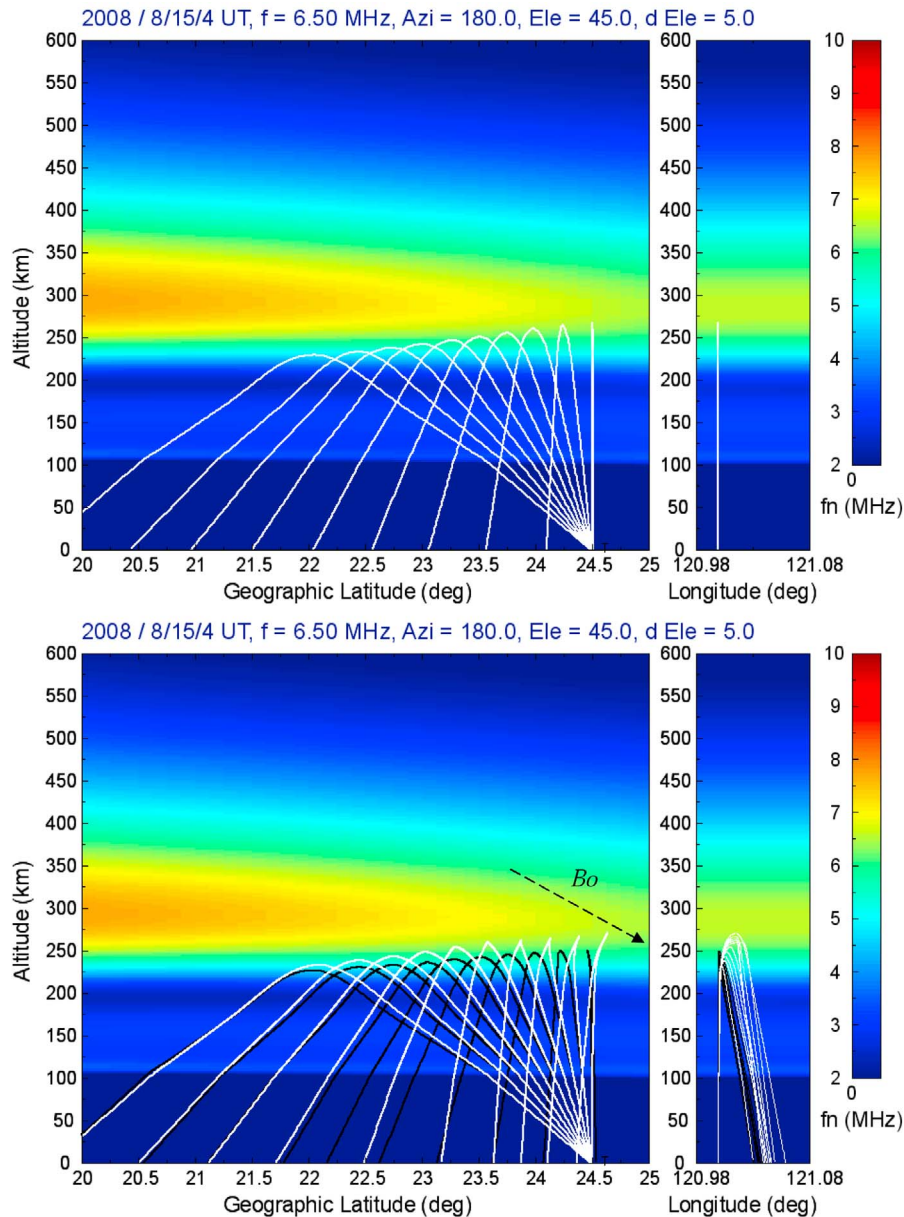


**Figure 3.** Ray-tracing paths with various launch elevation angles from  $90^\circ$  down to  $45^\circ$  in a step of  $5^\circ$ : (top) zero magnetic field and horizontal  $N_e$  gradient and (bottom) including both magnetic field and horizontal  $N_e$  gradient. The resulting raypaths are projected on to both the y-z (meridional and vertical) and x-z (longitudinal and vertical) planes, and the background imaging colors represent the modeling plasma frequencies from the TWIM.

magnetic field. Meanwhile, in the cases of Figure 3 (top) the propagations are essential two dimensional on the meridional and vertical plane. In contrast to the cases of Figure 3 (bottom), when the horizontal and transverse  $N_e$  gradient effect are included, the rays move out of the meridional and vertical plane, and off-great circle paths

arise for both o- and x-mode propagation. In Figure 3 (bottom), the ordinary rays with  $90^\circ$ ,  $85^\circ$ , and  $80^\circ$  launch elevation angles and the extraordinary raypath with  $90^\circ$  launch elevation angle have sharp corners and never becomes horizontal at the level of reflection. *Poeverlein* [1948] discovered the sharp-corner phenomenon known

**Table 1.** The Ray-Tracing Parameter Values of Reflection Height ( $h_r$ ), True Path ( $S$ ), Phase Path ( $P$ ), and Group Path ( $P'$ ) in Figure 3 (Top)

	90°	85°	80°	75°	70°	65°	60°	55°	50°	45°
$h_r$	267.0	264.9	261.1	256.3	251.7	247.2	242.8	238.5	234.2	230.1
$S$	537.0	534.0	540.0	546.0	558.0	579.0	603.0	633.0	663.0	726.0
$P$	457.2	456.0	462.7	472.8	487.6	510.5	536.3	569.6	604.1	665.2
$P'$	728.9	696.5	718.5	687.1	678.7	686.1	699.4	718.0	736.6	799.5

as the “spitze.” As shown in Figure 3 (bottom), these rays of ordinary waves both of the upward and downward ray directions are perpendicular to the Earth’s magnetic field at the reflection levels, and the reflection levels are at  $X = 1$ , i.e., the plasma frequency is equal to the radio frequency, and with small incidence angles. For the extraordinary ray with 90° launch elevation angle, the upward and downward ray directions at the reflection level ( $X = 1 - Y$ ) are parallel to the Earth’s magnetic field. As further descriptions of Figure 3 (top) and the o-mode wave propagations in Figure 3 (bottom), Tables 1 and 2, respectively, list the values of ray-tracing parameters including reflection height, true path, phase path, and group path. As expected in both cases, the reflection height decreases when the elevation angle decreases, and the true path is larger than the phase path but less than the group path. The path differences for cases where the horizontal  $N_e$  gradients exist and induce off-great circle propagations could approach more than 10 km for some rays. The ray-tracing analyses and three-dimensional  $N_e$  maps on the TWIM are available at “<http://isl.csr.sr.ncu.edu.tw/>” hosted by the Center for Space and Remote Sensing Research, National Central University, Taiwan.

[11] *Rogers et al.* [2001] assessed the potential use of radio tomography in HF ray-tracing applications and compared synthesized oblique ionograms by the SMART ray-tracing algorithms [*Norman and Cannon*, 1997] with experimental oblique ionograms. In this study we also simulate synthetic vertical ionograms by ray tracing on the TWIM and compare the results with experimental ionograms obtained by the dynasonde at Chung-Li (24.97°N, 121.19°E), Taiwan. The dynasonde is also referred by NOAA as the medium and high frequency (MF/HF) radar for ionospheric sounding. It can transmit sets of radio pulse at designed frequencies and measure complex amplitudes of ionospheric echoes and envelope group delay to 5  $\mu$ s resolution, i.e., 0.75 km in one-way range measurements. Meanwhile, the manipulation of echo data using the interference technique of spaced antennas enables derivation of the direction of wave arrival and wave polarization allowing the determination of ordinary or extraordinary mode signals by different

sense of wave vector rotation. The variation of the group range of reflection  $h'(f)$  as a function of radio frequency is the fundamental ionosonde data product and the records from these measurements are known as ionograms. The Chung-Li dynasonde routinely does sweep-frequency sounding and provides one ionogram every fifteen minutes. Synoptic ionospheric measurements derived from ionograms have provided valuable information both for radio propagation work and for studies related to the physical characteristics of the ionosphere. In this paper, an automatic tracing and scaling algorithm incorporating a fuzzy segmentation technique [*Tsai and Berkey*, 2000] has been applied to the ionograms obtained from the Chung-Li dynasonde. And thus, a fuzzy linking between echoes in chosen segments can be identified and used to determine the primary trace that characterizes ionospheric reflection and is further automatically scaled for ionospheric parameters.

[12] We have traced and simulated the rays vertically reflected from the ionosphere once, i.e., one-hop vertical soundings, at sweeping radio frequencies on a TWIM modeled ionosphere. The ionospheric soundings have been simulated from 0600 to 1800 LT on 14 November 2008, at the Chung-Li site. Figure 4 shows one sample comparison of ray-traced, synthetic ionogram with experimental ionogram, where the synthetic or experimental and ordinary or extraordinary echoes (and/or signals) are shown in different colors. The group ranges of synthetic ionogram are determined by the half of group paths described in the last section. To quantify the agreement between the synthetic and observed ionogram traces, two scale parameters of  $foF2$  (the ordinary-mode/o-mode critical frequency of the F2 layer) and  $h'oF2$  (the minimum o-mode group range of reflection at the F2 layer) are used. We do not include the E layer scale parameters because the Chung-Li transmitting antenna does not perform well at low radio frequencies and there are few normal E layer echoes from the observed ionograms. Figure 5 shows the temporal profiles of  $foF2$  and  $h'oF2$  from both of synthetic and experimental ionograms on 14 November 2008. The results show the RMS differences of 1.02 MHz and 21.9 km for  $foF2$  and  $h'oF2$ , respectively, between synthetic and experimental ionograms. The most errors of synthetic  $foF2$  and  $h'oF2$  are

**Table 2.** The Ray-Tracing Parameter Values of Reflection Height ( $h_r$ ), True Path ( $S$ ), Phase Path ( $P$ ), and Group Path ( $P'$ ) for the o-Mode Wave Propagations in Figure 3 (Bottom)

	90°	85°	80°	75°	70°	65°	60°	55°	50°	45°
$h_r$	271.5	267.6	264.9	262.8	260.5	254.8	249.2	244.1	239.3	233.9
$S$	550.7	541.7	537.8	538.9	547.7	564.6	598.0	627.8	666.5	722.8
$P$	462.3	461.1	462.9	467.6	477.2	497.6	533.2	565.9	607.1	665.6
$P'$	753.0	714.4	687.2	677.8	681.8	670.9	688.6	706.8	737.0	786.3

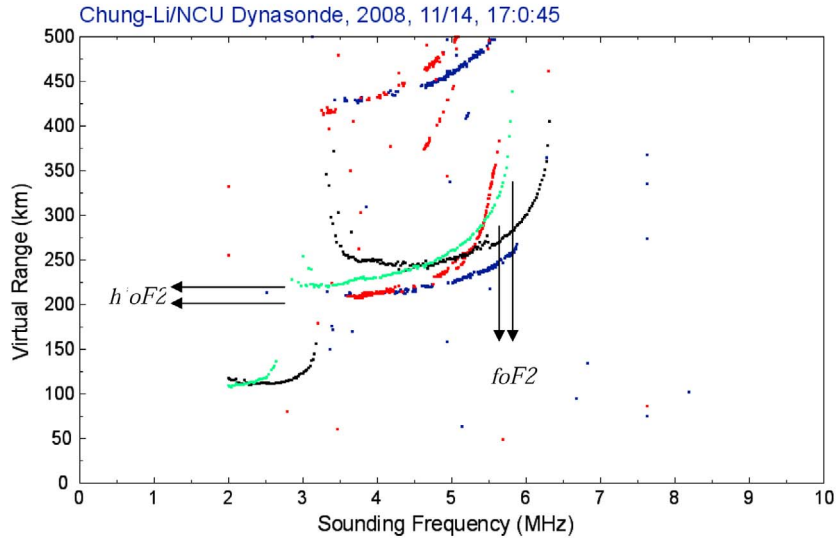


**Figure 4.** An example of comparison between experimental ionogram and synthetic ionogram at Chung-Li, Taiwan. Red, blue, green, and black dots show the experimental o-mode, experimental x-mode, synthetic o-mode, and synthetic x-mode echoes, respectively. The two scale parameters ( $foF2$  and  $h'oF2$ ) of ionograms are indicated.

caused by mismatch of the TWIM to the actual ionosphere. The TWIM was developed to model large-scale and statistical  $N_e$  variations only and could produce errors on short scale and/or duration variations. It can also be seen

that better matches of  $foF2$  and  $h'oF2$  at local times before 10 A.M. Some errors of synthetic  $h'oF2$  are caused by mismatches of  $foE$  (the E layer critical frequency) and/or

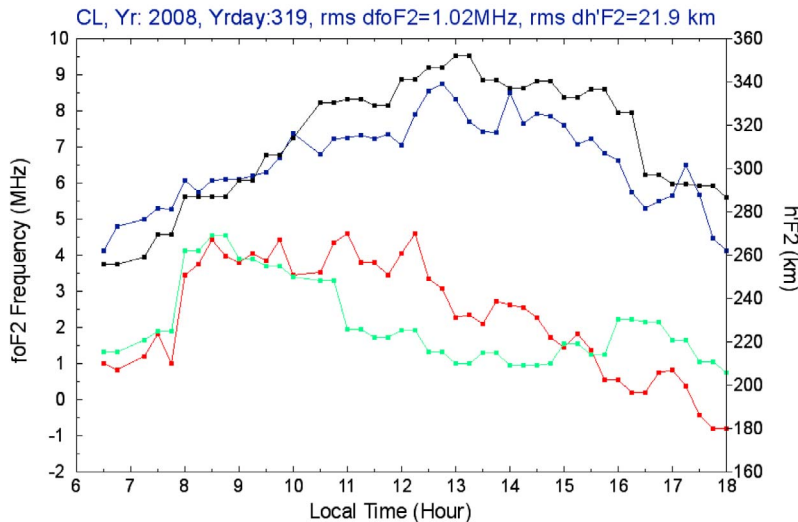


**Figure 5.** The  $foF2$  and  $h'oF2$  temporal profiles from experimental ionograms and synthetic ionograms on 14 November 2008, and at Chung-Li, Taiwan. Blue, black, red, and blue dots and lines show the experimental  $foF2$ s, synthetic  $foF2$ s, experimental  $h'oF2$ s, and synthetic  $h'oF2$ s, respectively.

$f_oF1$  (the F1 layer critical frequency) from the TWIM but not shown in this study.

## 5. Concluding Remarks

[13] An algorithm has been developed that can trace radio rays on a numerical ionospheric model of TWIM constructed from the F3/COSMIC data. The TWIM is intended to model large-scale and statistical  $N_e$  variations. It provides three-dimensional  $N_e$  distributions with vertically fitted  $\alpha$ -Chapman layers that have distinct F2, F1, E, and D layers, for which surface spherical harmonics approaches were used to represent the  $\alpha$ -Chapman layer parameters. The continuity of  $N_e$  and its derivatives is maintained in this model which allows practical schemes for providing reliable radio propagation prediction and electrostatic field determination. It has been shown that the stepped ray tracing described here allows for the inclusion of horizontal  $N_e$  gradients and the three dimensional Earth's magnetic field along the ray. Ray parameters such as the ground range, phase path, group path, and the reflection height are readily obtained. Comparisons of ray-traced, synthetic ionograms with experimental ionograms from the Chung-Li dynasonde have also shown the reliability of ray tracing on the TWIM.

[14] There are several areas in which the current ray-tracing algorithm could be improved. The most important is to improve the accuracy of  $N_e$  specification. The TWIM has been developed to model large-scale and statistical  $N_e$  variations, and thus increasing its temporal and spatial resolutions could provide better  $N_e$  specification which in turn will improve ray-tracing accuracy. Next, the centered-dipole field which is used as approximation to the geomagnetic field is sufficient for many purposes, but, for very accurate ray-tracing, the magnetic field can be replaced by a more complete representation on spatial resolution. Future works should also include the effect of electron collision and wave amplitudes estimation.

[15] **Acknowledgments.** This work has been supported by projects 98-NSPO(B)-IC-FA07-01(I), NSC98-2111-M-008-013-MY3, and NSC97-2111-M008-008-024-MY2.

## References

- Anderson, D. N., J. M. Forbes, and M. Codrescu (1989), A fully analytic ionospheric model (FAIM), *J. Geophys. Res.*, *94*, 1520.
- Appleton, E. V. (1932), Wireless studies of the ionosphere, *J. Inst. Electr. Eng.*, *71*, 642–650.
- Bennett, J. A., P. L. Dyson, and R. J. Norman (2004), Progress in radio ray tracing in the ionosphere, *Radio Sci. Bull.*, *300*, 81–91.
- Bremmer, H. (1949), *Terrestrial Radio Waves*, Elsevier, New York.
- Budden, K. G. (1952), The theory of the limiting polarization of radio waves reflected from the ionosphere, *Proc. R. Soc. London, Ser. A*, *215*, 215–233.
- Davis, H. F. (1989), *Fourier Series and Orthogonal Functions*, Dover, Mineola, N. Y.
- Försterling, K. (1942), Über die Ausbreitung elektromagnetischer Wellen in einem magnetisierten Medium bei senkrechter Inzidenz, *Hochfrequenztech. Elektroakust.*, *59*, 10–22.
- Hajj, G. A., L. C. Lee, X. Pi, L. J. Romans, W. S. Schreiner, P. R. Straus, and C. Wang (2000), COSMIC GPS ionospheric sensing and space weather, *Terr. Atmos. Oceanic Sci.*, *11*(1), 235–272.
- Hartree, D. R. (1931), The propagation of electromagnetic waves in a refracting medium in a magnetic field, *Proc. Cambridge Philos. Soc.*, *27*, 143–162.
- Haselgrove, J. (1955), Ray theory and a new method for ray tracing, in *The Physics of the Ionosphere*, edited by A. C. Stickland, pp. 355–364, Phys. Soc., London.
- Hines, C. O. (1951), Wave packets, the Poynting vector, and energy flow: 1. Nondispersive (anisotropic) homogeneous media, *J. Geophys. Res.*, *56*, 63–72.
- Jones, R. M. (1966), A three dimensional ray-tracing computer program, *ESSA Tech. Rep.*, *IER 17-ITS*, 17.
- Jones, W. B., and R. M. Gallet (1962), The representation of diurnal and geographic variations of ionospheric data by numerical methods, *Telecommun. J.*, *29*, 129.
- Kelso, J. M. (1964), *Radio Ray Propagation in the Ionosphere*, McGraw-Hill, New York.
- Lawrence, R. S., and D. J. Posakony (1961), A digital ray-tracing program for ionospheric research, in *Space Research*, vol. 2, edited by H. C. van de Hulst, C. de Jager, and A. F. Moore, pp. 258–276, North-Holland, Amsterdam.
- Norman, R. J., and P. S. Cannon (1997), A two-dimensional analytic ray tracing technique accommodating horizontal gradients, *Radio Sci.*, *32*(2), 387–396.
- Poevlerlein, H. (1948), Strahlwege von Radiowellen in der Ionosphäre (I), *Sitzungsberichte der Bayerischen Akademie der Wissenschaften*, 175–201.
- Poevlerlein, H. (1949), Strahlwege von Radiowellen in der Ionosphäre (II), *Zeitschrift für angewandte Physik*, 517–525.
- Reilly, M. H. (1991), Upgrades for efficient three-dimensional ionospheric ray tracing: Investigation of HF near vertical incidence sky wave effects, *Radio Sci.*, *26*(4), 971–980.
- Rocken, C., Y.-H. Kuo, W. Schreiner, D. Hunt, S. Sokolovskiy, and C. McCormick (2000), COSMIC system description, *Terr. Atmos. Oceanic Sci.*, *11*(1), 21–52.
- Rogers, N. C., C. N. Mitchell, J. A. T. Heaton, P. S. Cannon, and L. Kersley (2001), Application of radio tomographic

- imaging to HF oblique incidence ray-tracing, *Radio Sci.*, 36, 1591–1598.
- Rydbeck, O. E. H. (1944), On the propagation of radio waves, *Trans. Chalmers Univ. Technol.*, 34, 1–170.
- Schreiner, W. S., S. V. Sokolovskiy, C. Rocken, and D. C. Hunt (1999), Analysis and validation of GPS/MET radio occultation data in the ionosphere, *Radio Sci.*, 34(4), 949–966.
- Shinn, D. H., and H. A. Whale (1952), Group velocities and group heights from the magnetoionic theory, *J. Atmos. Terr. Phys.*, 2, 85–105.
- Tricomi, F. G. (1985), *Integral Equations*, 238 pp., Dover, Mineola, N. Y.
- Tsai, L.-C., and F. T. Berkey (2000), Ionogram analysis using fuzzy segmentation and connectedness techniques, *Radio Sci.*, 35(5), 1173–1186.
- Tsai, L.-C., C. H. Liu, and T. Y. Hsiao (2009a), Profiling of ionospheric electron density based on the FormoSat-3/COSMIC data: Results from the intense observation period experiment, *Terr. Atmos. Oceanic Sci.*, 20(1), 181–191, doi:10.3319/TAO.2007.12.19.01 (F3C).
- Tsai, L.-C., C. H. Liu, T. Y. Hsiao, and J. Y. Huang (2009b), A near real-time phenomenological model of ionospheric electron density based on GPS radio occultation data, *Radio Sci.*, 44, RS5002, doi:10.1029/2009RS004154.

---

J. Y. Huang and L.-C. Tsai, Center for Space and Remote Sensing Research, National Central University, Chung-Li 320, Taiwan. (lctsai@csrsr.ncu.edu.tw)

C. H. Liu, Academia Sinica, Taipei 115, Taiwan.